ACS APPLIED MATERIALS & INTERFACES

Research Article

www.acsami.org

Rectification Behavior of PATP Self-Assembled on ZnO Microrod Arrays

Shengjiang Fang, Chunxiang Xu,* Zhulin Jin, Fengyu Sheng, Zengliang Shi, Yueyue Wang, and Gangyi Zhu

State Key Laboratory of Bioelectronics, School of Electronic Science and Engineering, Southeast University, Nanjing, 210096, People's Republic of China

ABSTRACT: A rectifying hybrid junction was fabricated by the self-assembly of 4-aminothiophenol (PATP) on well-aligned ZnO microrod arrays. Good rectification behavior was obtained from the device of Al/ZnO/PATP/Al. The electron transport at the ZnO/PATP interface was investigated systematically by experimental observation and theoretical simulation. X-ray photoelectron spectroscopy (XPS) analysis confirmed the strong binding between PATP and ZnO via S−Zn bonds. The effective energy barrier and ideality factor of the rectifying diode were estimated by the current−voltage (I−V) measurement and thermionic emission theory. The molecule dipole effect on work function was studied through energy band theory. Theoretical calculation results based on density functional theory (DFT) also indicated a significant dipole, caused by the anchoring effect of PATP, resulting in the changes of surface electronic characteristics of ZnO.

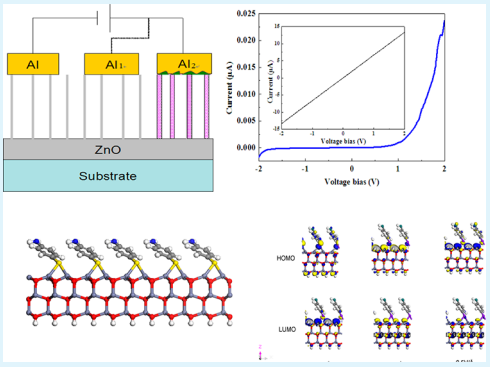

KEYWORDS: *molecular rectifier, ZnO/PATP interface, electron transport, self- assembly, molecule dipole effect*

1. INTRODUCTION

Since Aviram and Ratner initially proposed molecular rectifiers using single molecules as active elements in 1974,[1] molecular electronics are considered to be a promising way to overcome the physical limitations of conventional microelectronics.[2−6] In particular, the design and construction of functional molecular devices on metal-oxides or semiconductors have inspired great interest.[7−16] For instance, dipolar molecule phosphonic acids have been used to control the surface properties of indium tin oxide (ITO) to optimize device performance in both organic light-emitting diodes (OLED) and organic photovoltaic cells.[13,14] Meanwhile, with regard to application, some reports have attempted to develop the rectifying diodes by assembling the organic molecules on Si and GaAs semiconductor surfaces via carboxylate bonds.[15,16] Similarly, molecular control over the barrier height is more effective with an ionic semiconductor (ZnO).[17] The high isoelectric point (IEP ≈ 9.5)[18] and c-axis polarity of ZnO are beneficial to immobilize many organic molecules on its surface through electrostatic adsorption and self-assembly.[19] Moreover, the electronic properties of microstructural and nanostructural ZnO is easily tuned by surface modification.[20] PATP, as a typical dipolar "D-π-A" type molecule with a highly polarizable conjugated π-system has been revealed to have potential application in molecular electronics.[21−24] For example, directional charge transfer at the ZnO/PATP interface has been demonstrated by surface-enhanced Raman spectroscopy (SERS).[22] Even so, the theoretical research and the expected rectification devices have not been reported.

In this paper, a rectifying diode was fabricated based on self-assembling PATP on ZnO microrod arrays through S−Zn bonds. The hybrid device presents good rectification behavior. The mechanism, especially the molecule dipole effect on electron transfer process at the ZnO/PATP interface is systematically investigated in experiments and theory.

2. EXPERIMENTAL SECTION

The ZnO microrods were grown on quartz substrates using the vapor-phase transport (VPT) technique, similar to our previous report.[25,26] A mixture of ZnO and graphite powder with a mass ratio of 1:1 was placed into a small quartz boat as source materials, and a quartz slice covered the quartz boat; then, they were put into a horizontal furnace that was heated up to 1050 °C. ZnO microrod arrays were obtained on the quartz substrate after reaction for 10 min. The morphology and microstructure of the product were examined using scanning electron microscopy (SEM) on a ZEISS Ultra Plus system and X-ray diffraction (XRD) on a MAC Science system (Model MXPAHF).

The self-assembly was carried out by immersing half of an as-grown ZnO sample into a 0.2 mM PATP solution in ethanol at room temperature for 24 h. After PATP adsorption, the sample was removed from the reactor and rinsed three times with ethanol and deionized water, respectively, and finally dried under a nitrogen (N_2) stream. The Al/ZnO/PATP/Al hybrid

Received: January 26, 2013
Accepted: April 2, 2013
Published: April 2, 2013

junction was fabricated by evaporating aluminum on the top of the vertically aligned ZnO microrod arrays in a vacuum of 5×10^{-6} Torr. X-ray photoelectron spectroscopy (XPS) was then employed to characterize the chemical state of the elements (e.g., Zn, S, and N) on the PATP-treated ZnO microrod surface, which were calibrated with the binding energy of the C 1s core level. The molecular layer is removed by sputtering the sample, using an argon-ion beam with an energy of 4 keV, a current of 15 mA, and an atmospheric pressure of 1×10^{-2} Pa. The estimated thickness of the monolayered PATP is ~5 Å, according to experiments and the calculations of previous reports.[27] The sample was cleavaged gradually by sputtering for 600 s at a rate of 0.5 Å/min, and the element distribution was analyzed using XPS signals recorded at various depths. The elemental amounts were estimated using Gaussian−Lorentz decomposition peaking at the intrinsic binding energy of the related element, based on a linear background. The schematic diagram of the structure and the current−voltage (I−V) measurement of the device are given in Figure 1. The pink

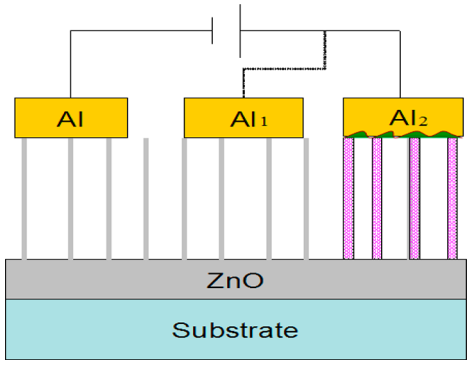

Figure 1. Schematic diagram of the structure and the current−voltage (I−V) measurement of the device.

color represents the ZnO microrod with the PATP molecule anchored on its surface, and the gray color represents the ZnO seed layer, which is located between the two white dotted lines shown in the SEM image in Figure 2a; the wavy layer marked with the purple color represents the PATP molecule converging at the interface. A voltage bias is applied on the two yellow blocks, which denotes the Al electrodes with the positive direction is from the right one (Al1or Al2) to the left one. I−V characteristics were collected in the voltage scan mode between the two Al electrodes at room temperature, using a semiconductor analyzer (Keithley, Model SCS 4200) with an integration time of 20 ms.

Theoretical calculation based on density functional theory (DFT) was performed using the DMol3 code.[28,29] A uniform generalized gradient approximation (GGA) with the PW91 form was adopted.[29] Double numerical basis sets including polarization functions on all atoms (DNP) were used in the calculations.[30,31] The initial atomic structure of ZnO (002) layer was established from bulk ZnO. Three layers of Zn−O were set on ZnO cluster, in which the bottom two layers of Zn−O were fixed and the bottom O atoms were passivatied by H atoms. The lattice constant of ZnO is $a = b = 6.498$ Å, $\alpha = \beta = 90°$, $\gamma = 60°$. Another 20 Å vacuum region was added at the top surface to get rid of the interlayer interactions.

3. RESULTS AND DISCUSSION

Morphology and Microstructure of ZnO Microrod Arrays. The SEM images of as-grown ZnO microrods in Figure 2a and 2b reveal the general morphology of vertically well-aligned ZnO microrod arrays. The diameters and lengths of the microrods are ~1 and 28 μm, respectively. The energy-dispersive spectrometry (EDS) spectrum in Figure 2c shows that the ZnO microrod prepared via the VPT method is rich in zinc, which is beneficial to chemical adsorption of PATP on the top surface of ZnO microrods. The XRD test result shown in Figure 2d reveals the high orientation of ZnO microrods along the [0002] direction. The XRD pattern of ZnO microrod can be indexed as hexagonal ZnO, which is consistent with the values in the standard card, and no impurity was observed. The intensity of the ZnO (0002) peak is much stronger than other ZnO peaks, which indicates that the (0002) plane might be the primary face of the microrods.

PATP-Assembled ZnO Microrod Surface. The PATP-assembled ZnO microrod surface was characterized by XPS. Figure 3 illustrates the representative binding modes, although some signals are not very strong, because of the low concentration of PATP. The XPS signal of the S 2p core level in Figure 3a is composed of two peaks of S $2p_{3/2}$ at 161.1 eV and S $2p_{1/2}$ of 162.4 eV origin from the S−Zn covalent bond.[32] The N 1s peak appears at 399.2 eV in the spectrum shown in Figure 3b, which is from ph-NH_2.[33] No other peak was observed, which indicates that the N element is not linked to ZnO. As shown in Figure 3c, two separate peaks of Zn $2p_{3/2}$, located at 1021.8 and 1020.6 eV, are consistent with the intrinsic binding energy of Zn corresponding to Zn−O and Zn−S bonds. The weak signal corresponding to S−Zn bond demonstrated the small amount of PATP on ZnO surface. Furthermore, the atomic concentration ratio of sulfur and nitrogen (S/N) is measured over time using a sputtering procedure, as shown in Figure 3d. It is obvious that the ratio of S/N generally shows an upward trend, which implies that the orientation of the molecular layer may be sulfur at the bottom and amino at the top. Especially at 420 s, the S/N ratio jumps to a much higher value that corresponds to the combination point of S−Zn bond. As a result, the majority of the molecules roughly stand neatly on the ZnO.

Current−Voltage (I−V) Characteristic. Current−voltage characteristics are carried out on the diode with PATP modified as shown in Figure 4. Good current-rectifying characteristics were observed with a low turn-on voltage of ~0.5 V. The rectification ratio, which is defined as $I(1.5\ \text{V})/I(-1.5\ \text{V})$, is ~47, indicating that the Al/ZnO/PATP/Al hybrid junction is well-formed. As shown in the inset, such phenomenon is not found in the diode without PATP modification: a linear I−V curve with a conductance of 6.67 μS, which represents a perfect ohmic contact between Al and ZnO, was given.

To view electron transport across the hybrid junctions, a thermionic emission model is used to study the potential barrier:[16]

$$I = I_0\{\exp\left[\frac{q(V - IR_s)}{nkT}\right] - 1\} \quad (1)$$

where V is the applied bias, q the electron charge, k the Boltzmann constant, T the temperature, R_s the diode series resistance, I_0 the saturation current for a zero barrier, and n the diode ideality factor, which also known as the quality factor or, sometimes, the emission coefficient. The ideality factor (n)

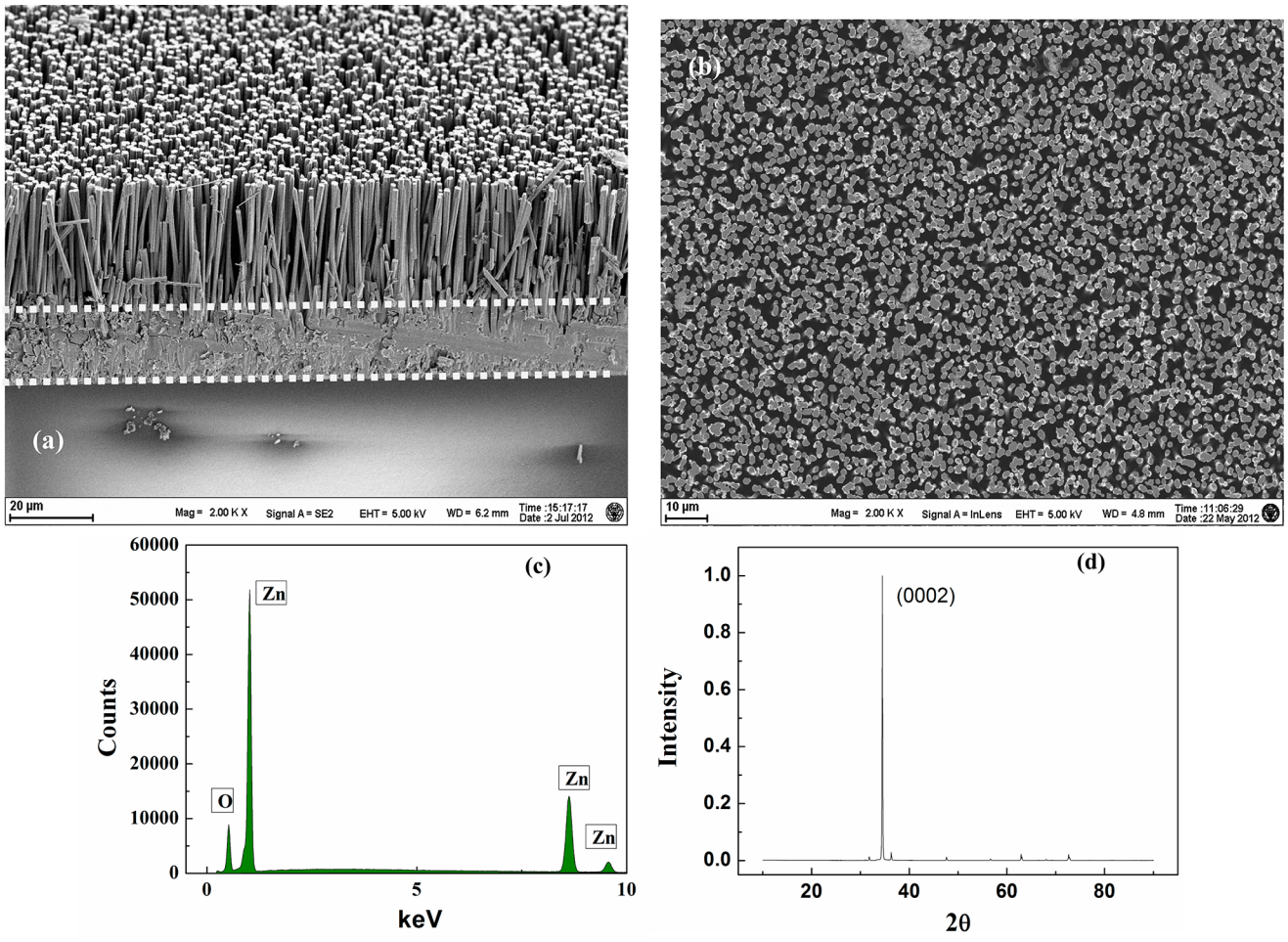

Figure 2. SEM image ((a) side view and (b) top view) of a vertically aligned VPT-grown ZnO microrod array; (c) EDS data spectrum and (d) XRD patterns of the ZnO microrods array.

varies from 1 to 2, depending on the fabrication process and semiconductor material; in many cases, it is assumed to be ∼1 (thus, the notation "n" is omitted), so the value of n indicates how closely a diode follows the ideal diode equation. For $V \gg nkT/q$, the "−1" term can be neglected, and a plot of ln I vs V should be linear above 0.1 V at room temperature. The barrier height (φ_b) can be extracted from the following equation:[34]

$$I_0 = AA^* T^2 \exp\left(\frac{-q\varphi_b}{kT}\right) \quad (2)$$

where A is the contact area (A = 0.002 cm^2), T the temperature (T = 298 K), φ_b the effective barrier height, and A^* the effective Richardson constant (A^* = 32 A cm^{-2} K^{-2} for ZnO), which accounts for the transmission probability through the interface. By fitting the measured ln I versus voltage plot between 0.1 V and 0.4 V, ln I_0 can be obtained from the intercept of the linear (semilogarithmic) fit. The barrier height φ_b extracted from eq 2 is 0.885 eV. In order to get the diode ideality factor, eq 1 is rewritten in the form of the current density J (as $J = I/A$) and the −1 term is neglected, and then the following equation is obtained:

$$V = R_s AJ + n\varphi_b + \left(\frac{nkT}{q}\right)\ln\left(\frac{J}{A^* T^2}\right) \quad (3)$$

By calculating the differential of eq 3, we get

$$\frac{dV}{d(\ln J)} = R_s AJ + \frac{nkT}{q} \quad (4)$$

According to the measured I−V data, we redraw a curve of V with respect to ln J when the series resistance R_s closes to zero; we can get a straight line, and the n value can be obtained from the slope. In this way, we get a value of n = 4.615. Obviously, the forward current transport in the Al/ZnO/PATP/Al hybrid junction is separate from the pure thermionic emission for which n = 1. The fitting was reasonably good, especially in the bias direction in which current flow is favorable. Thus, it is reasonable to attribute the high ideality factor to the interfacial energy barrier induced by the chemisorbed PATP layer on ZnO surface. The following study is concentrated on the PATP molecule effects on the energy band and the electronic characteristics of ZnO.

Energy Band Study. Band bending can be introduced by the adsorption of the molecule on the ZnO surface. It was reported by Lin et al., who showed that the formation of Zn−S bonds induced a 0.71 eV shift in the valence band maximum (VBM) to a lower binding energy, leading to an increase in the surface band bending.[35]

As an ionic n-type semiconductor, the majority carriers in ZnO are electrons, that is, the density of free electron carriers (n_e) is higher than that of hole carriers (n_h). The PATP acts as acceptors depleted the surface electron states and reduced the free carrier density; negative charges exist at the surface and

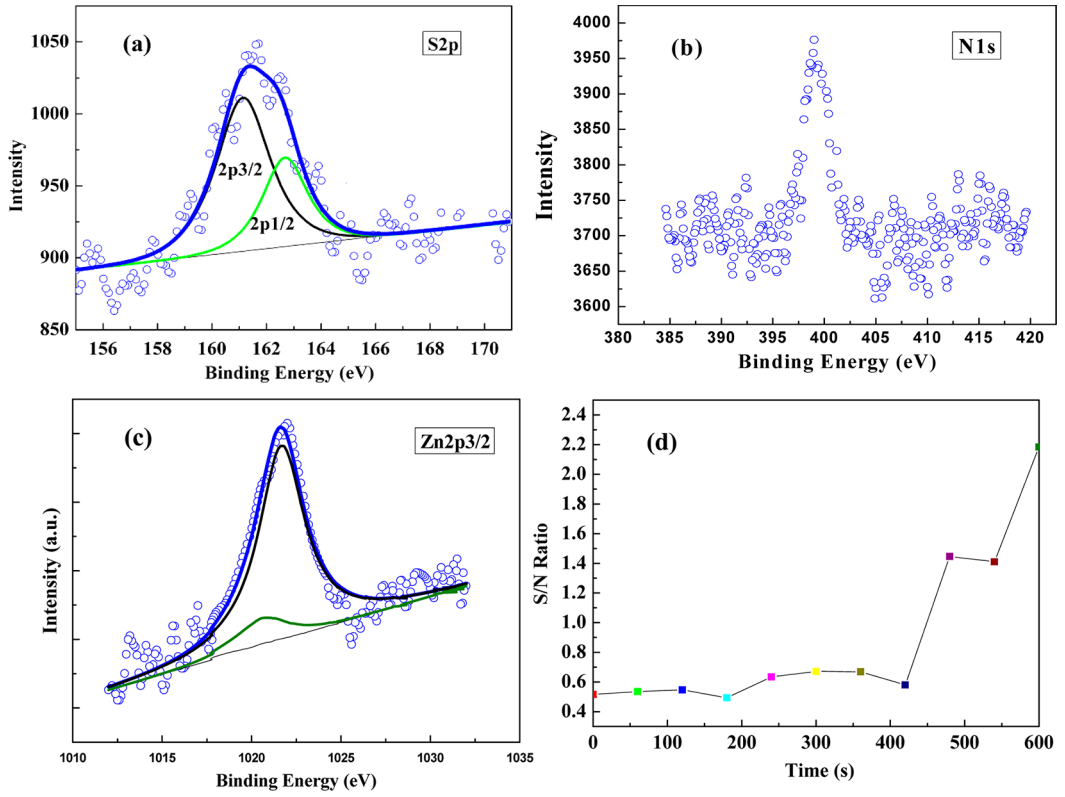

Figure 3. XPS spectra of ZnO microrods functioned by PATP: (a) Gaussian−Lorentz decomposition of the XPS S 2p core level peaks, (b) the N 1s peak at 399.2 V, and (c) Gaussian−Lorentz decomposition of the XPS Zn $2p_{3/2}$ peak for peak separation. (d) Element concentration data ratio of sulfur to nitrogen (S/N).

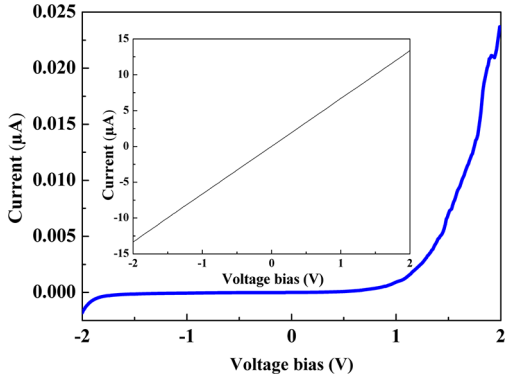

Figure 4. *I*−*V* characteristics of the Al/ZnO/PATP/Al diode at room temperature. The inset shows the plot of Al/bulk ZnO/Al without PATP modification.

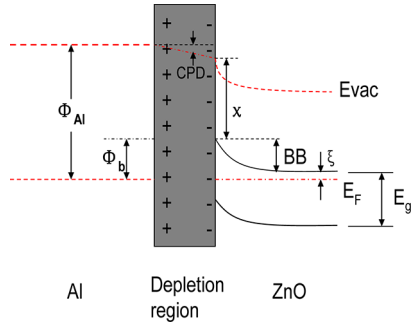

Figure 5. Schematic description of molecular effect on the barrier height and contact potential difference of the junction that was added to the dipolar molecule layer.

positive charges accumulate near the surface, causing a decrease of n_e and an increase of n_h. A space charge region called the "depletion layer" then emerged, which introduces an upward band bending, as illustrated in Figure 5. The effect of the PATP molecular layer at the interface can be taken as a dipole layer, which is analogous to a parallel-plate capacitor. Moreover, the potential energy drop over it (φ_{dip}) can be estimated by[16]

$$\varphi_{dip} = \frac{q\mu \cos\theta}{A\varepsilon\varepsilon_0} \quad (5)$$

where μ is the molecular dipole moment (C m) (which has an average tilt θ from the normal), A the area per molecule (m^2), ε_0 the permittivity of vacuum, and ε the dielectric constant of the dipole layer.[36,37] The role of the potential energy dropping over the surface dipole layer is to change the native electron affinity or work function to an effective one. The work function difference between metal and semiconductor is called the contact potential difference (CPD), which was introduced by PATP modification in the present case, as shown in Figure 5. CPD and φ_b can be defined as

$$\mathrm{CPD} = \varphi_{Al} - \varphi_{ZnO} = \varphi_{Al} - (\chi + \mathrm{BB} + \xi) \quad (6)$$

$$\varphi_b = \varphi_{Al} - \chi \quad (7)$$

where φ_{Al} and φ_{ZnO} are the work function of Al and ZnO, respectively; χ is the electron affinity of ZnO; BB is the band bending; and $\xi = E_{CB} - E_F$ for *n*-type ZnO. As shown in Figure 5, the introduced dipole layer leads to a decrease of the electron affinity and work function of ZnO, and further results in the increase of CPD and barrier height. With these changes,

dx.doi.org/10.1021/am400349w | ACS Appl. Mater. Interfaces 2013, 5, 3298−3303

directional charge transfer occurred in this system, and finally induced asymmetry of the $I-V$ curve.

DFT Simulation. The DFT simulation was carried out before and after PATP modification on the ZnO surface. The initial distance between PATP and the ZnO is set to be 3.0 Å and PATP is perpendicular to the ZnO plane. After geometry optimization, the PATP is titled at an angle of 30° and the S atom links with two Zn atoms, as shown in Figure 6a. The

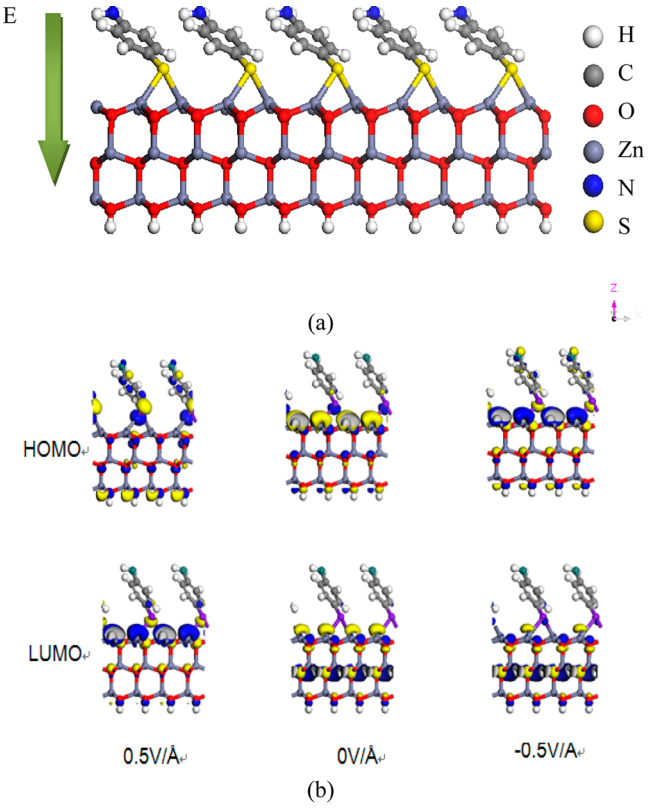

Figure 6. Density functional theory (DFT) calculation results of ZnO/PATP composites: (a) the view of the optimized ZnO/PATP composite and (b) side views of the localized electronic density distribution of LUMO (bottom) and HOMO (top) states for a neutral ZnO/PATP composite with electric fields of −0.5, 0, and 0.5 V/Å. The wave function has a negative value for the yellow symbols and a positive value for the blue symbols.

corresponding local electron density distributions of the ZnO/PATP composite with electric fields of 0, −0.5, and 0.5V/Å, respectively, are given in Figure 6b. Without an electric field, the electron density of the highest occupied molecular orbital (HOMO) state is mainly localized at the interface between ZnO and PATP, while the distribution of the lowest unoccupied molecular orbital (LUMO) states is evenly localized at the interface and the inside of ZnO cluster. The dipole associated with the molecule−substrate bond is determined by charge rearrangement upon formation of the substrate-adsorbed molecular monolayer.[38] The electron density distributions, which converged at the interface of ZnO and PATP, indicate that a significant interface dipole was introduced by the S−Zn bond. Moreover, the changes of the electron density also indicate a significant polarization dependent on electric field direction. When a positive electric field of 0.5 V/Å is applied, the electron density distribution of LUMO converges at the interface while the HOMO state is predominantly localized over the PATP segment. It is interesting that the opposite electron density distribution occurs when a negative electric field of −0.5 V/Å is applied. Table 1 clearly shows that, with the change of the electric field

Table 1. Changes of Calculated Electronic Parameters of the Neutral ZnO/PATP Composite Compress to the Bare ZnO and Dependent on the Applied Electric Field (EF), Including the Changes of the Work Function (ΔWF), the HOMO−LUMO Gap (ΔE_g), the Fermi Energy Level (ΔE_f), and the Dipole Moment ($\Delta\mu_z$) Perpendicular to the Surface

EF (V/Å)	ΔWF (eV)	ΔE_g (eV)	ΔE_f (eV)	$\Delta\mu_Z$
−0.5 (vs 0)	+1.14	0.013	−0.775	
0.5 (vs 0)	−1.36	−0.348	0.931	
0 (vs bare)	−0.65		+0.65	−0.68

direction, the HOMO and LUMO gap change correspondingly. Meantime, the change of work function for the PATP-modified ZnO surface is −0.65 eV (compares with bare ZnO). Especially, the work function was reduced when the electric field increased to a forward bias of 0.5 V/Å, and rose at the negative bias of −0.5 V/Å. It means the electrons in the composite are easy to escape as soon as a positive electric field is applied. Therefore, the opposite changes in electron density distributions, Fermi level, work function, and band gap indicates that electrons in the ZnO/PATP composite are more likely to escape from the potential barrier to the right electrode (Al2) shown in Figure1. Besides, the charge transport of the diode can qualitatively be explained by considering the effect of bond dipole (BD) on alignment of the Fermi energy level of the ZnO substrate and the metal electrode. Because of the anchoring thiol group, the surface dipole of the ZnO substrate decreased (−0.68 eV for the perpendicular component of the dipole moment (μ_z)) and the local charge was rearranged. A negative BD is developed with the formation of this covalent bond, leading to a decrease in the electrostatic potential at the interface between the anchoring group and the ZnO substrate. Thus, the Fermi level of the ZnO will be increased by the reaction between thiol and zinc. Meanwhile, the positive BD from the amino group will decrease the Fermi energy level of the Al electrode. This alignment of the Fermi level induced by the anchoring effect makes the electron tunneling through the HOMO more favorable, because the HOMO of this molecular diode is much closer to the Fermi energy level of the Al electrode. Therefore, when the voltage bias was applied, because of the contrary BD effects between the amino groups and thiol anchoring groups, the rectifying behavior was observed.

4. CONCLUSIONS

In conclusion, a "D-π-A" type molecule PATP has been conjugated onto covalently functionalized ZnO microrod arrays by a simple self-assembly method to construct a microhybrid device with good rectification behavior. The electron transport and rectifying mechanism were studied by experimental investigation and DFT simulations. The XPS and simulation results revealed that the molecule was linked to ZnO through S−Zn covalent bonds rather than by physical adsorption. Current−voltage characterizations taken before and after PATP molecule anchored on the ZnO microrods suggested how the molecule PATP affected the electronic characteristics of ZnO microrods. The energy band and simulation study illustrated

that a series of electronic parameters of the device changed after PATP anchoring onto the ZnO surface, which provided the possible source of rectifying behavior. Further study of the simulation reveals the molecule dipole effect on—and the directional charge transfer at—the interface of ZnO/PATP of this molecule diode.

AUTHOR INFORMATION

Corresponding Author

*Tel.: 86-25-83790755. E-mail: xcxseu@seu.edu.cn.

Notes

The authors declare no competing financial interest.

ACKNOWLEDGMENTS

This work is supported by NSFC (No. 61275054), RFDP (No. 20110092130006), and JSIS (No. BE2012164).

REFERENCES

(1) Aviram, A.; Ratner, M. A. *Chem. Phys. Lett.* **1974**, *29*, 277−283.
(2) Song, H.; Reed, M. A.; Lee, T. *Adv. Mater.* **2011**, *23*, 1583−1680.
(3) Moth-Poulsen, K.; Bjornholm, T. *Nat. Nanotechnol.* **2009**, *4*, 551−556.
(4) Yaffe, O.; Scheres, L.; Puniredd, S. R.; Stein, N.; Biller, A.; Lavan, R. H.; Shpaisman, H.; Zuilhof, H.; Haick, H.; Cahen, D.; Vilan, A. *Nano Lett.* **2009**, *9*, 2390−2394.
(5) Coskun, A.; Spruell, J. M.; Barin, G.; Dichtel, W. R.; Flood, A. H.; Botros, Y. Y.; Stoddart, J. F. *Chem. Soc. Rev.* **2012**, *41*, 4827−4859.
(6) Lakshmi, S.; Dutta, S.; Pati, S. K.. *J. Phys. Chem. C* **2008**, *112*, 14718−14730.
(7) Roth, K. M.; Yasseri, A. A.; Liu, Z. M.; Dabke, R. B.; Malinovskii, V.; Schweikart, K. H.; Yu, L. H.; Tiznado, H.; Zaera, F.; Lindsey, J. S.; Kuhr, W. G.; Bocian, D. F. *J. Am. Chem. Soc.* **2003**, *125*, 505−517.
(8) Delcamp, J. H.; Yella, A.; Holcombe, T. W.; Nazeeruddin, M. K.; Gratzel, M. *Angew. Chem., Int. Ed.* **2013**, *52*, 376−380.
(9) Duan, X. F.; Huang, Y.; Lieber, C. M. *Nano Lett.* **2002**, *2*, 487−490.
(10) Collier, C. P.; Mattersteig, G.; Wong, E. W.; Luo, Y.; Sampaio, J.; Raymo, F. M.; Stoddart, F. M.; Heath, J. R. *Science* **2000**, *289*, 1172−1175.
(11) Collier, C. P.; Jeppesen, J. O.; Luo, Y.; Perkins, J.; Wong, E. W.; Heath, J. R.; Stoddart, J. F. *J. Am. Chem. Soc.* **2001**, *123*, 12632−12641.
(12) Liao, K. C.; Ismail, A. G.; Kreplak, L.; Schwartz, J.; Hill, I. G. *Adv. Mater.* **2010**, *22*, 3081−3085.
(13) Hotchkiss, P. J.; Li, H.; Paramonov, P. B.; Paniagua, S. A.; Jones, S. C.; Armstrong, N. R.; Bredas, J. L.; Marder, S. R. *Adv. Mater.* **2009**, *21*, 4496.
(14) Hotchkiss, P. J.; Jones, S. C.; Paniagua, S. A.; Sharma, A.; Kippelen, B.; Armstrong, N. R.; Marder, S. R. *Acc. Chem. Res.* **2012**, *45*, 337−346.
(15) Lenfant, S.; Krzeminski, C.; Delerue, C.; Allan, G.; Vuillaume, D. *Nano Lett.* **2003**, *3*, 741−746.
(16) Vilan, A.; Ghabboun, J.; Cahen, D. *J. Phys. Chem. B* **2003**, *107*, 6360−6376.
(17) Salomon, A.; Berkovich, D.; Cahen. *Appl. Phys. Lett.* **2003**, *82*, 1051−1053.
(18) Gu, B. X.; Xu, C. X.; Zhu, G. P.; Liu, S. Q.; Chen, L. Y.; Li, X. S. *J. Phys. Chem. B* **2009**, *113*, 377−381.
(19) Gu, B. X.; Xu, C. X.; Yang, C.; Liu, S. Q.; Wang, M. L. *Biosens. Bioelectron.* **2011**, *26*, 2720−2723.
(20) Lao, C. S.; Li, Y.; Wong, C. P.; Wang, Z. L. *Nano Lett.* **2007**, *7*, 1323−1328.
(21) Zhou, Q.; Li, X. W.; Fan, Q.; Zhang, X. X.; Zheng, J. W. *Angew. Chem., Int. Ed.* **2006**, *45*, 3970−3973.
(22) Sun, Z. H.; Wang, C. X.; Yang, J. X.; Zhao, B.; Lombardi, J. R. *J. Phys. Chem. C* **2008**, *112*, 6093−6098.
(23) Farcau, C.; Potara, M .; Leordean, C .; Boca, S .; Astilean, S. *Analyst* **2013**, *138*, 546−552.
(24) Ward, D. R.; Halas, N. J.; Ciszek, J. W.; Tour, J. M.; Wu, Y. P.; Nordlander, P.; Natelson, D. *Nano Lett.* **2008**, *8*, 919−924.
(25) Zhu, G. P.; Xu, C. X.; Zhu, J.; Lv, C. G.; Cui, Y. P. *Appl. Phys. Lett.* **2009**, *94*, 051106.
(26) Zhu, G. Y.; Xu, C. X.; Lin, Y.; Shi, Z. L.; Li, J. T.; Ding, T.; Tian, Z. S.; Chen, G. F. *Appl. Phys. Lett.* **2012**, *101* (4), 041110.
(27) Rosario-Castro, B. I.; Fachini, E. R.; Hernandez, J.; Perez-Davis, M. E.; Cabrera, C. R. *Langmuir* **2006**, *22*, 6102−6108.
(28) Delley, B. *J. Chem. Phys.* **2000**, *113*, 7756−7764.
(29) Delley, B. *Phys. Rev. B* **2002**, *66*, 155125.
(30) Perdew, J. P.; Wang, Y. *Phys. Rev. B* **1992**, *45*, 13244−13249.
(31) Delley, B. *J. Chem. Phys.* **1996**, *100* (15), 6107−6110.
(32) Kim, S. H.; Kim, H. K.; Seong, T. Y. *Appl. Phys. Lett.* **2005**, *86*, 022101.
(33) Jones, C.; Sammann, E. *Carbon* **1990**, *28*, 509.
(34) Liu, J. S.; Shan, C. X.; Li, B. H.; Zhang, Z. Z.; Yang, C. L.; Shen, D. Z.; Fan, X. W. *Appl. Phys. Lett.* **2010**, *97*, 251102.
(35) Lin, Y. J.; Sai, C. L. *J. Appl. Phys.* **2006**, *100*, 113721.
(36) Kronik, L.; Shapira, Y. *Surf. Sci. Rep.* **1999**, *37*, 1−206.
(37) Iwamoto, M.; Mizutani, Y.; Sugimura, A. *Phys. ReV. B* **1996**, *54*, 8186−8190.
(38) Aqua, T.; Cohen, H.; Sinai, O.; Frydman, V.; Bendikoy, T.; Krepel, D.; Hod, O.; Kronik, L.; Naaman, R. *J. Phys. Chem. C* **2011**, *115*, 24888−24892.